

3-D Underflow of a Sluice Gate at a Channel Inlet; Experimental Results and CFD Simulations

Francesco Calomino and Agostino Lauria*

Department of Civil Engineering, Università della Calabria, Via P. Bucci 42b, 87036, Rende, Cosenza, Italy

*Corresponding author's Email: agostino.lauria@unical.it

ABSTRACT: The underflow of a sluice gate is well known when the gate is set into a channel of the same width (2-D underflow), while no studies are found in the literature when the gate is flush with the wall of the tank or reservoir upstream to the channel (3-D underflow). Experimental and numerical investigations were carried out to study the flow in this case, in a small range of relative openings, considering three wall slopes, and obtaining an equation for the discharge coefficient. Afterwards, numerical simulations were performed by means of a CFD (Computational Fluid Dynamics) model, following the RANS approach and based on a finite-volume computational code. Comparison of experimental and numerical results showed that the simulations predict accurately the flow behaviour; thereafter discharge coefficients in a more extended range of relative openings were computed for use in the practice.

Keywords: Channel Inlet, Sluice Gate, 3-D Underflow, Discharge Coefficients, CFD Simulations.

ORIGINAL ARTICLE
Received 24 Apr. 2014
Accepted 25 Jun. 2014

INTRODUCTION

Flow at a channel inlet controlled by gate

The flow at a channel inlet is in many cases controlled by a sluice gate, set at the downstream end of a tank and flush with the wall limiting it. This is the case of weirs for flood control purposes, in which the river flow may be regulated by a sluice gate, and of irrigation channels derived by a shallow reservoir. Even though these works are largely diffused, their hydraulics is still not well known. The aims of this paper are:

1. experimentally studying the inlet of a rectangular channel, controlled by a sluice gate of the same width, flush with the vertical or sloping wall of the tank or reservoir supplying water to the channel (3-D underflow), in order to obtain the discharge coefficients in a small range of relative openings;
2. simulating the flow by means of a CFD (Computational Fluid Dynamics) software;
3. providing an equations for the discharge coefficients in a wider field than that allowed by the experimental observations.

As one can understand, there are some simplifying assumptions, with which the designer can easily comply. With this in mind, the problem geometry is essentially shown in Figure 1a and Figure 1b, where a and b are the dimensions of the rectangular orifice under the gate, θ is the angle between the tank wall and the horizontal, h is the water level into the tank of width B . The sluice gate is set at the intersection between the tank wall and the channel walls and it has a sharp edge, while the bottom of the tank or reservoir is set on the same horizontal plan of the channel inlet.

The flow is eminently three-dimensional, since the vein under the sluice gate is contracted both on the vertical and the horizontal directions. At the channel inlet

one can observe two oblique stationary waves strongly affecting the flow, as well a vertical vortex at a short distance upstream of it.

Experimental tests, together with 3-D numerical simulation, allowed us to sufficiently understand the flow behaviour and to obtain a formula an equation valid in a small range of relative openings. Numerical simulations allowed us to validate the CFD model and to compute discharge coefficients in a in a wider field.

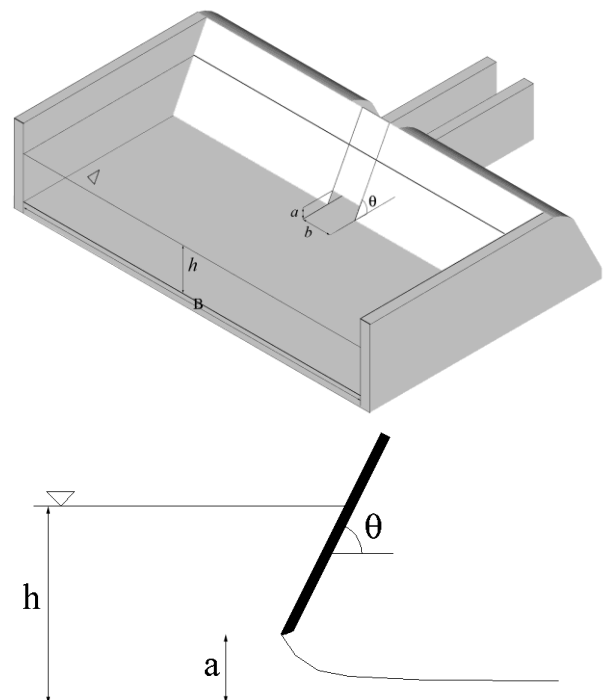


Figure 1. a) Schematic of channel inlet controlled by sluice gate; b) Detail of underflow of the gate

Underflow of a sluice gate set into a rectangular channel

Even though the case we are studying presents a three-dimensional contracted vein, it can be approached by the equation used for bi-dimensional flow under a sluice gate set into a rectangular channel of the same width. As it is well known, even though in a simplified way, in practice the orifice formula can be used, where the discharge Q is varying with the square root of the water depth h :

$$Q = C_d \cdot a \cdot b \cdot \sqrt{2 \cdot g \cdot h} \quad (1)$$

a being the opening height, b its width, h the water depth into the tank or reservoir measured from the bottom of orifice, and C_d the discharge coefficient.

The theory and experiments leading to C_d values can be found in the works of Cisotti (1908), Gentilini (1941), Marchi (1953) and Montes (1997). Henderson (1966) summarized the experimental data observed by Henry (1950), and, more recently, Rajaratnam and Subramanya (1967) and Nago (1984) provided experimental values for C_d . Roth et al. (1999) carried out the most complete study on the topic, by means of tests on a rectangular flume and scale effect analysis. Among other results, the Authors showed the presence of a ridge upstream to the gate, forming where the horizontal velocity components are almost equal to zero; moreover, they observed a recirculation zone in the upper part of the flow, upstream to the gate, affecting the contraction of the vein and the overall discharge, and two oblique stationary waves at the beginning of the channel, as a consequence of two vortices forming at the sluice gate sides.

Figure 2 shows the experimental data mentioned above, giving C_d as a function of the relative opening a/h ; according to Roth et al. (1999), some of the literature data present higher C_d values because of viscosity and surface tension effects.

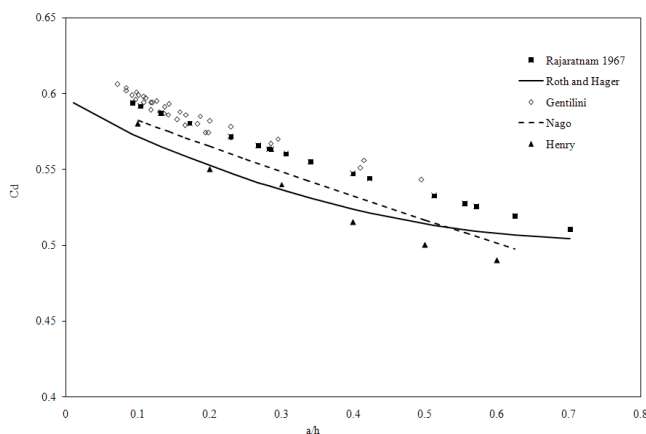


Figure 2. Literature values of C_d for bi-dimensional flow under a sluice gate

A few Authors use a numerical approach, among which Kim (2005, 2007), who by means of a CFD model carried out the study of discharge coefficients for a sluice gate, and Akoz et al. (2009), who, using the same model, compared the experimental observations of velocity and water level with the values obtained from numerical simulations using $k - \epsilon$ turbulence model. Oskuyi et al. (2012), developed two equations, linear and nonlinear, to

determine discharge coefficient by using dimensional analysis and linear and nonlinear regression analysis, for both free and submerged flow conditions.

MATERIAL AND METHODS

Dimensional analysis

With respect to Figure 1, we can assume a function F of the discharge Q and the other geometrical variables h , b , a , as defined above, the angle between wall and horizontal plane θ , gravity acceleration g , water density ρ , kinematic viscosity ν and surface tension σ , that is:

$$F(Q, h, b, a, \theta, g, \rho, \nu, \sigma) = 0$$

We neglected the effect of the tank or reservoir width, B , provided that it be sufficiently larger than b . From Π theorem, we get to:

$$\Phi \left(\frac{Q}{a^{5/2} \cdot \sqrt{g}}, \frac{b}{a}, \frac{h}{a}, \frac{a^{3/2} \cdot \sqrt{g}}{\nu}, \frac{\rho \cdot g \cdot a^2}{\sigma}, \theta \right) = 0 \quad (2)$$

where Φ is a generic function, the parameter b/a is the shape ratio, a/h is the relative opening, and

$$Re = \frac{a^{3/2} \cdot \sqrt{g}}{\nu} \quad (3)$$

and

$$We = \frac{\rho \cdot g \cdot a^2}{\sigma} \quad (4)$$

are the Reynolds and Weber gate numbers, respectively.

When the liquid is the same and the temperature is constant, Re and We depend on each other and vary with the gate opening only, as shown by Raju (1984).

So, we obtain

$$\Phi \left(\frac{Q}{a^{5/2} \cdot \sqrt{g}}, \frac{b}{a}, \frac{h}{a}, Re, \theta \right) = 0$$

and, bearing in mind eq. (1), we can write

$$C_d = \Phi \left(\frac{a}{h}, \frac{b}{a}, Re, \theta \right) \quad (5)$$

Carrying out the tests in conditions where viscosity and surface tension do not affect the flow, C_d becomes a function of geometrical variables only:

$$C_d = \Phi \left(\frac{a}{h}, \frac{b}{a}, \theta \right) \quad (6)$$

RESULTS

The experiments were carried out in a 4.00 m long, 1.20 wide and 0.25 m deep horizontal rectangular tank; the wall at its downstream extremity could be set at three values of the angle θ , equal to 45° (1/1), $63,4^\circ$ (2/1) and 90° (vertical wall), it was divided in two parts and an orifice was created using a sluice gate flush with the plane to which the upstream faces of the two middles belonged. Figure 3 shows a plan view of the experimental set-up, you can find more details in Calomino et al. (2007). The sluice gate was made up of a PVC sheet 1.0 cm thick and it had a sharp edge. Three values of the orifice width b were studied, that is 86 mm, 106 mm and 142 mm, with the gate openings of 50, 60 and 70 mm. Preliminary tests following the approach suggested by Roth et al. (1999),

allowed us to observe that for openings a greater or equal to 5 cm, the scale effects could be avoided, since C_d became independent of Re . The laboratory circuit fed the tank, by gradually opening a valve; the flow was collected at the downstream exit of the orifice in a small horizontal flume and conveyed by a funnel and to a 100 mm PVC pipe, where it was recorded by means of an ultrasonic flowmeter. A Thomson weir at the upstream extremity made it possible to check the ultrasonic flowmeter, when the flow was steady. The Thomson weir was volumetrically calibrated with an accuracy of 1%. During

each test, the stage into the tank was recorded by means of a pressure transducer, with the tapping at 50 cm upstream of the orifice. Also a number of piezometric taps were in turn connected to the same pressure transducer, in order to get pressure measurements in 12 points of the tank. An electric point gauge allowed control of the pressure transducer measurement once steady conditions were achieved. Both flow and stage measurements were collected by an acquisition system at the frequency of 50 Hz, then stored into a computer and processed.

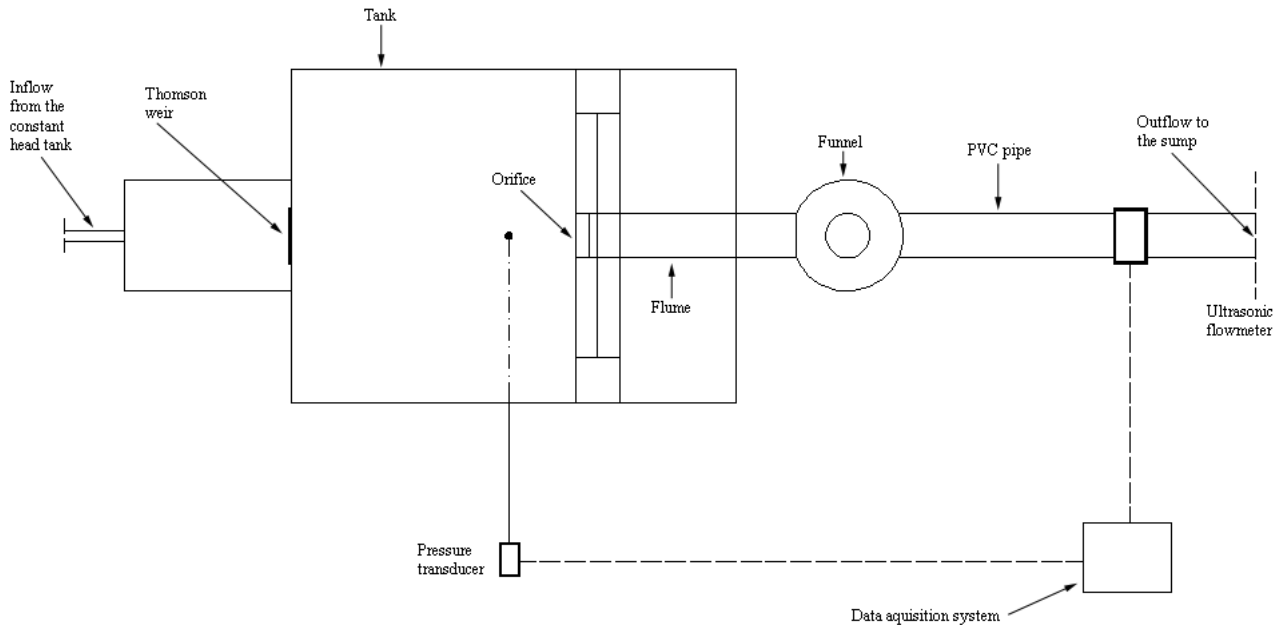


Figure 3. Sketch of experimental set-up

Once the steady state was achieved, discharge and water stage measurements were collected; moreover, for some tests, velocity values were collected close to the gate and along its axis with an acoustic doppler velocimeter (ADV). We carried out 27 tests with the steady flow discharge ranging from 3.50 l/s to 7.70 l/s. Since the uncertainty on discharge measurement, was considered $\pm 3.0\%$ and that on water stage measurement $\pm 1.0\%$, at the confidence level of 95,4%, the uncertainty affecting C_d was considered to be $\pm 3.5\%$ at the same confidence level, the experimental results are summarized in Table 1.

During the tests we observed the presence of a vertical vortex immediately upstream of the gate, shown in Figure 4a, instead of the two observed for sluice gates having the same width of the channel (Roth and Hager, 1999); moreover we observed the presence of two standing symmetrical oblique waves forming downstream of the gate, shown in Figure 4b.

Regression analysis was carried out using the experimental data, and the following equation was obtained

$$C_d = 0.322 \cdot \left(\frac{a}{h}\right)^{-0.228} \cdot \left(\frac{b}{a}\right)^{-0.002} \cdot \theta^{0.064} \quad (7)$$

valid in the range $45^\circ < \theta < 90^\circ$, $0.28 \leq a/h \leq 0.56$, $1.23 \leq b/a \leq 2.84$, with determination coefficient $R^2=0.843$. Figure 5 shows the experimental and computed values of C_d , and these fall within the $\pm 3,5\%$ uncertainty band.

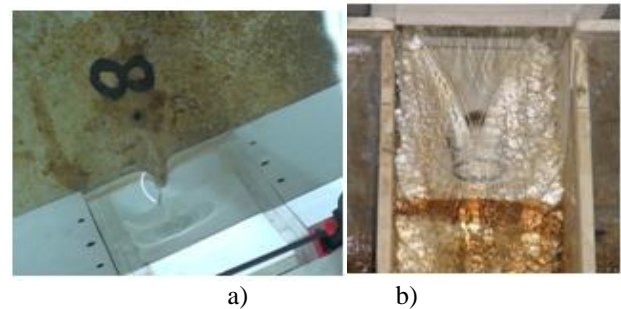


Figure 4. a) Vertical vortex immediately upstream to the gate; b) Symmetrical oblique waves downstream of the gate.

Since the influence of b/a and θ resulted to be not significant, by neglecting these variables we obtained the equation:

$$C_d = 0.404 \cdot \left(\frac{a}{h}\right)^{-0.27} \quad (8)$$

valid in the same range, with determination coefficient $R^2=0.732$; this equation can be assumed for the sake of simplicity, with uncertainty of $\pm 4,5\%$; the regression curve and uncertainty band are shown in Figure 6, where we show also Roth et al. (1999) equation for the 2-D sluice gate. The different behaviour is evident; it depends on the shape of the liquid surface downstream to the gate where two standing oblique waves appear.

Table 1. Experimental data

Test	θ (°)	a (mm)	b (mm)	h (mm)	Q (l/s)	b/a	a/h	C_d
T-01	90	50	142	176.10	7.40	2.84	0.28	0.56
T-02	90	60	142	148.60	7.70	2.36	0.4	0.53
T-03	90	70	142	122.20	7.50	2.03	0.57	0.49
T-04	90	50	106	142.00	4.90	2.12	0.352	0.55
T-05	90	60	106	156.40	6.00	1.76	0.385	0.54
T-06	90	70	106	180.10	7.60	1.51	0.389	0.54
T-07	90	50	86	152.50	4.20	1.72	0.33	0.57
T-08	90	60	86	151.50	4.80	1.43	0.40	0.54
T-09	90	70	86	154.00	5.50	1.23	0.45	0.53
T-10	63.4	50	142	144.06	6.30	2.84	0.35	0.53
T-11	63.4	60	142	156.30	7.60	2.36	0.38	0.51
T-12	63.4	70	142	142.00	7.40	2.03	0.54	0.47
T-13	63.4	50	106	148.70	4.70	2.12	0.34	0.52
T-14	63.4	60	106	147.50	5.50	1.76	0.41	0.51
T-15	63.4	70	106	148.40	6.10	1.51	0.47	0.48
T-16	63.4	50	86	131.00	3.60	1.72	0.38	0.52
T-17	63.4	60	86	144.60	4.30	1.43	0.41	0.50
T-18	63.4	70	86	152.80	5.10	1.23	0.46	0.49
T-19	45	50	142	109.00	5.20	2.84	0.46	0.50
T-20	45	60	142	141.50	7.20	2.36	0.42	0.51
T-21	45	70	142	125.90	7.40	2.03	0.56	0.47
T-22	45	50	106	117.30	4.10	2.12	0.43	0.51
T-23	45	60	106	144.62	5.40	1.76	0.41	0.50
T-24	45	70	106	154.60	6.30	1.51	0.45	0.49
T-25	45	50	86	125.10	3.50	1.72	0.40	0.52
T-26	45	60	86	136.00	4.20	1.43	0.44	0.50
T-27	45	70	86	140.30	4.80	1.23	0.50	0.48

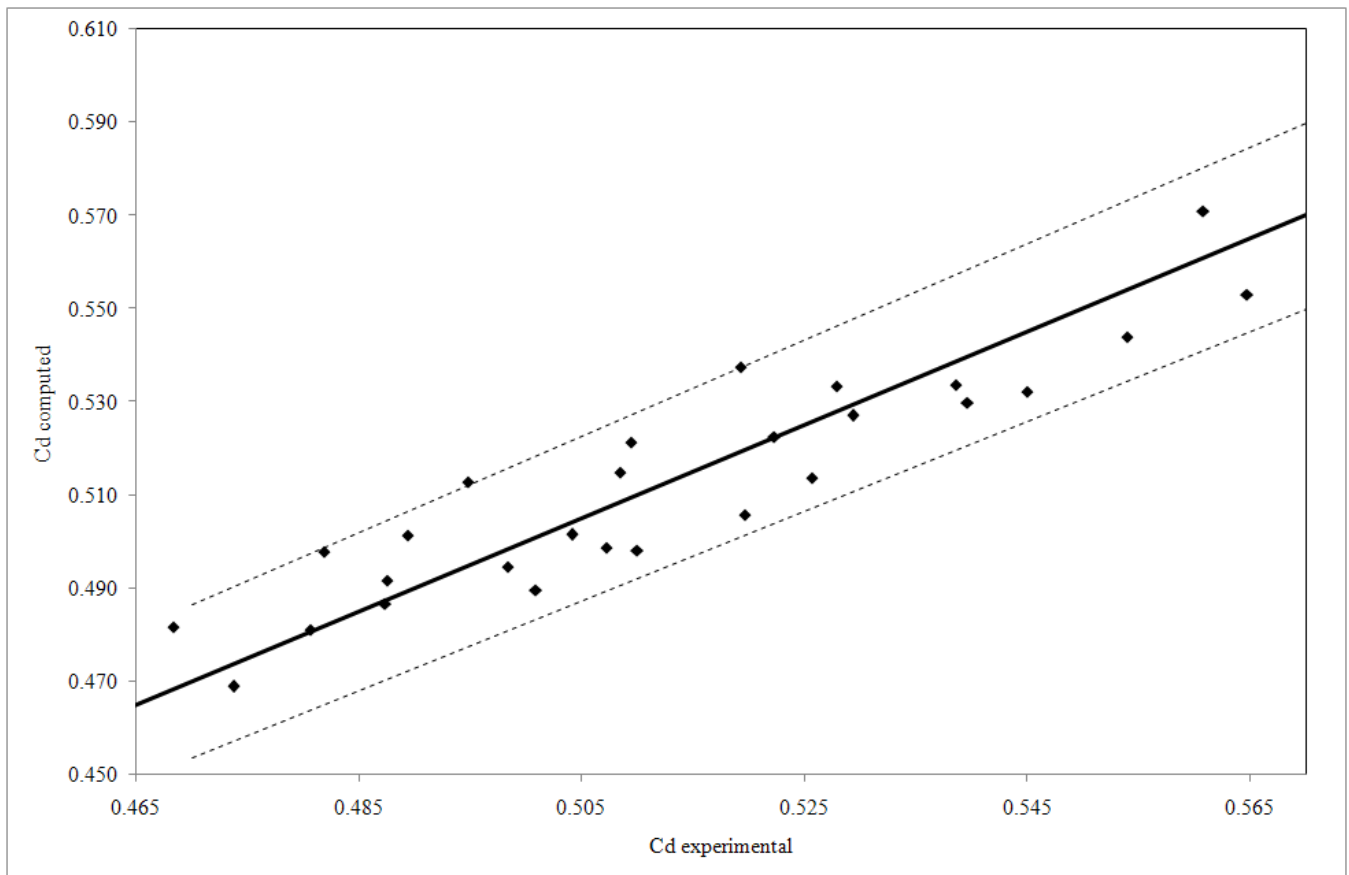


Figure 5. Eq (7) - Computed vs experimental C_d and $\pm 3.5\%$ confidence bound ($45^\circ < \theta < 90^\circ$, $0.28 \leq a/h \leq 0.56$, $1.23 \leq b/a \leq 2.84$)

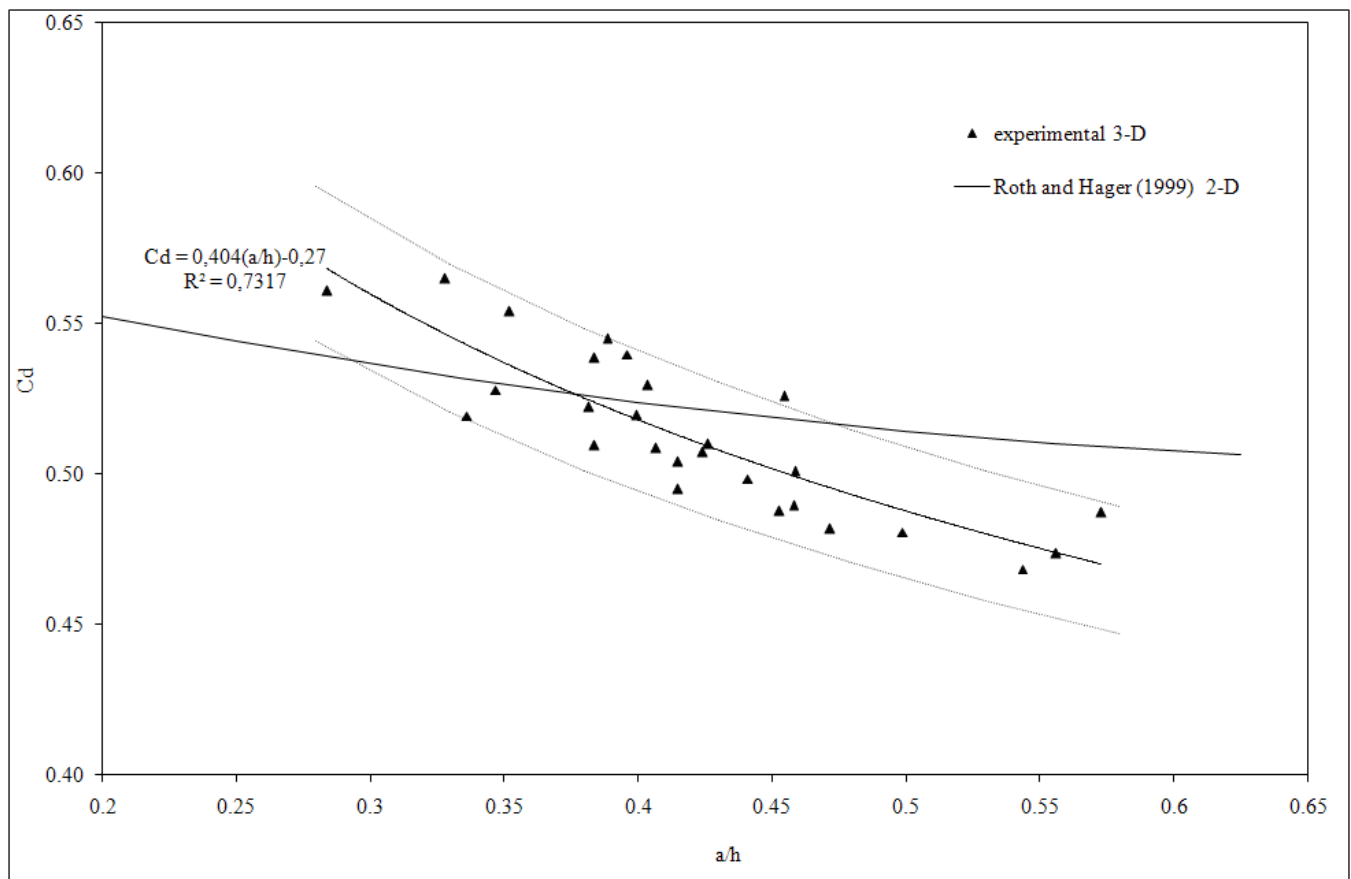


Figure 6. Eq (8) - Experimental and computed C_d values v/s a/h and $\pm 4.5\%$ uncertainty band ($45^\circ < \theta < 90^\circ$, $0.28 \leq a/h \leq 0.56$, $1.23 \leq b/a \leq 2.84$)

CFD simulations

A number of simulations were performed with the aim of extending the investigation field, after accurate calibration of the CFD model used. Flow3D® finite-volume computational code was used, in this code, the free-surface condition is handled with the VOF (Volume Of Fluid) method, as devised by Hirt et al. (1981) and the treating of the surface of solid objects is handled with the FAVOR™ (Fractional Area/Volume Obstacle Representation, see also Flow Science, 2004). The Reynolds-Averaged continuity and Navier-Stokes equations (RANS) were used to simulate the flow on a Eulerian structured fixed mesh. The time-marching procedure includes three main steps (Alfonsi et al., 2012):

i) evaluation of the velocity in each cell using the initial conditions (or previous-time-step values) for the advective pressures (and/or other accelerations), on the basis of appropriate explicit approximations of the governing equations;

ii) adjustment of the pressure in each cell to satisfy the continuity equation;

iii) updating of the fluid free surface to give the new fluid configuration based on the volume-of-fluid value in each cell.

In this work, the available solution scheme based on the Generalized Minimal Residual (GMRES) method has been used. The computing system used for the simulations includes 2 Intel Xeon 5660 processors, a maximum of 4 GB of RAM, and up to 0.5 TB of mass memory.

The geometry is composed by a rectangular tank 0.496 meters long and 0.400 meters wide and a rectangular horizontal channel 0.300 meter long.

The computational domain extends 0.496 m x 0.400 m x 0.300 m along the x (streamwise), y (spanwise) and z (vertical) directions, respectively.

The origin of the coordinate system (x, y,z) is located at the lower-left corner of the computational domain, as shown in Figure 7.

As what concerns the grid resolution, a number of tests were performed before reaching the final configuration of the grid, employing an increasing number of points, up to that we finally utilized. The results of these tests are outlined in Table 2. A three-dimensional computational volume of about 1.86×10^6 grid points has been set-up.

Table 2. Grid refinement progression for T-01

Parameters	Grid A	Grid B	Grid C	Grid D (final)
Nx	80	90	100	124
Ny	90	90	100	100
Nz	100	100	120	150
Δx min (m)	0.0062	0.0051	0.0049	0.0020
Δy min (m)	0.0044	0.0044	0.0040	0.0020
Δz min (m)	0.0030	0.0030	0.0020	0.0020
C_d	0.51	0.52	0.54	-
Err. Rel. To Grid D (%)	8.8	7.1	3.5	-

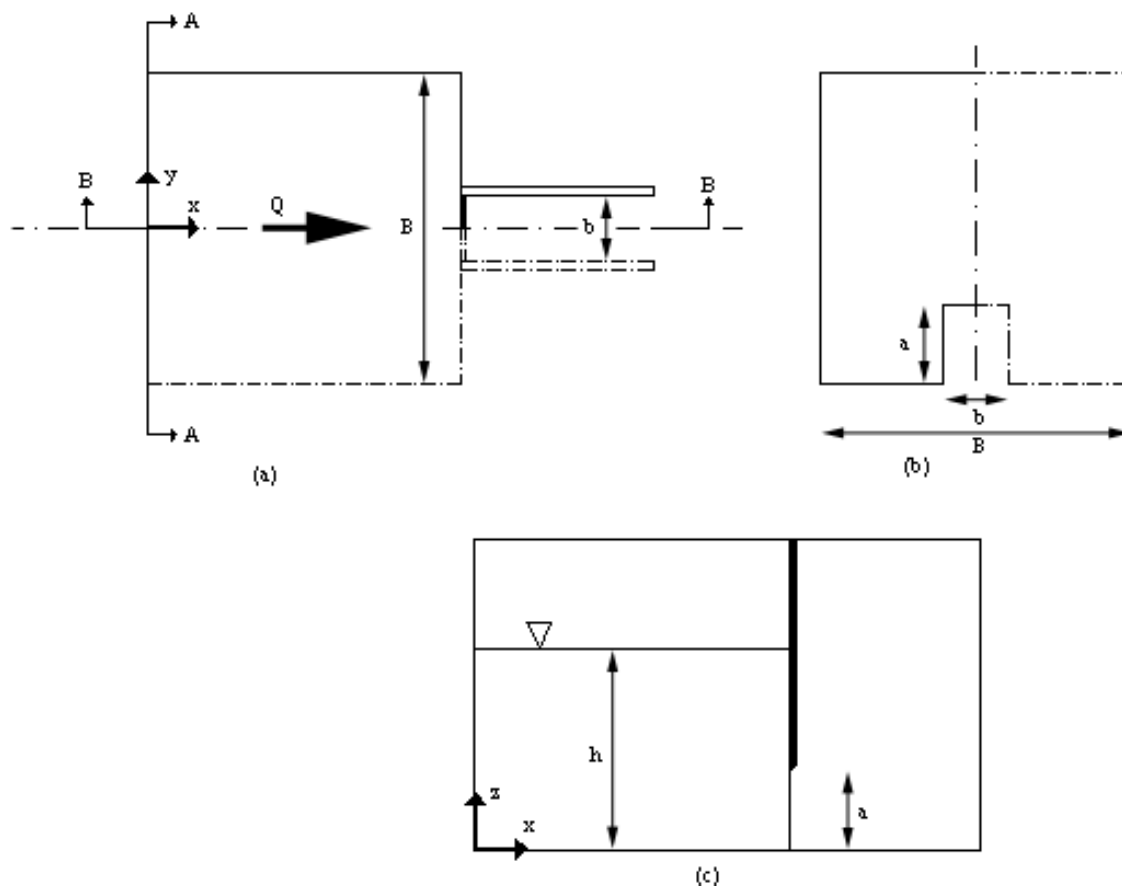


Figure 7. Computational domain and initial condition (dashed lines indicate that half of computational domain was not considered in the numerical model); a) plan view; b) A-A section, view from upstream; c) B-B section, lateral view

The minimum grid spacing was used in the vicinity of the sluice gate and it was equal to 2 mm while the maximum was used far from sluice gate and it was equal to 8 mm. The boundary conditions used for the computational domain are the followings; the no-slip (and zero wall-normal velocity) condition has been imposed on the x - y bottom plane and at the geometry external surface. To reduce the computational cost, the Symmetry condition has been imposed on the x - z left boundary plane and on the top of computational domain, on the y - z end-plane of the computing domain outflow conditions have been set, while the free-surface condition holds at the fluid surface. On the y - z inlet plane, constant fluid depth is imposed, equal to that observed in the experimental test to be simulated.

An initial condition of constant depth, equal to the experimental one we measured and equal to that imposed at y - z plane, was imposed in the portion of domain upstream of the gate, that is the fluid moves with an instantaneous opening of the gate at $t=0$.

Details on the implementation of numerical model are reported in Lauria (2008).

By means of the CFD model, 15 different configurations were simulated, obtaining for each of them the values of h and Q in steady-state conditions. The first 9 simulations were performed for the case with $\theta = 90^\circ$, both in the condition of inviscid fluid and viscous fluid. To simulate the condition with viscous fluid the RNG (Renormalization Group $k - \epsilon$) turbulence model was used, since it appears particularly suitable in cases like the one we studied (Akoz et al., 2009). Comparison of the

computations and experimental results showed a good accuracy of the numerical values of h (fluid depth) and Q (discharge), once a good grid refinement was achieved. Evaluation of energy losses was carried out, following the method used in Roth et al. (1999), showing very small losses compared to kinetic energy; this is why inviscid fluid conditions can simulate well the experimental results. With the computed values of Q and h , the discharge coefficients were obtained by eq. (1).

Figure 8 shows, for one of the tests, the computed velocities and those measured by means of ADV at different locations, at the distances upstream of the gate $x = 20, 40$ and 60 mm; the results show good agreement with experimental data.

The results of numerical simulations show the presence of two symmetrical oblique wavefronts, forming downstream of the gate, similarly to those observed in the experimental tests. Moreover, the model simulates enough well the recirculation zone upstream to the gate, typical of the underflow of a planar sluice gate, observed also by Roth et al. (1999). The limited computing resources we used did not allow us to simulate the vertical-axes vortex observed upstream to the gate. Since for the 9 tests simulated with angle $\theta=90^\circ$, both the conditions of inviscid and viscous fluid bring practically to the same results, we carried out afterwards 3 simulations with angle $\theta=45^\circ$ and 3 with angle $\theta=63,4^\circ$ for inviscid fluid only.

Assuming $\theta=45^\circ$ and $b/a = 2$, 3 more simulations were carried out for inviscid flow, in a range of gate openings $0,20 < a/h < 1$, larger than the experimental one and including cases that could not be observed by the

experimental set-up. Considering negligible the effect of (b/a) and θ , by regression analysis we obtained the equation

$$C_d = 0,707 e^{-0,7(a/h)} \quad (9)$$

valid in the range for $45^\circ \leq \theta \leq 90^\circ$, $0,2 < a/h < 1,0$, $1 \leq b/a \leq 2,84$ with determination coefficient $R^2=0,976$.

This equation is very close to eq. (8) obtained by experimental results in the range $0,28 < a/h < 0,56$; the regression curve is shown in Figure 9 together with the $\pm 4,5\%$ uncertainty band; the same figure shows Roth and Hager equation for the 2-D underflow, to underline the difference between the two.

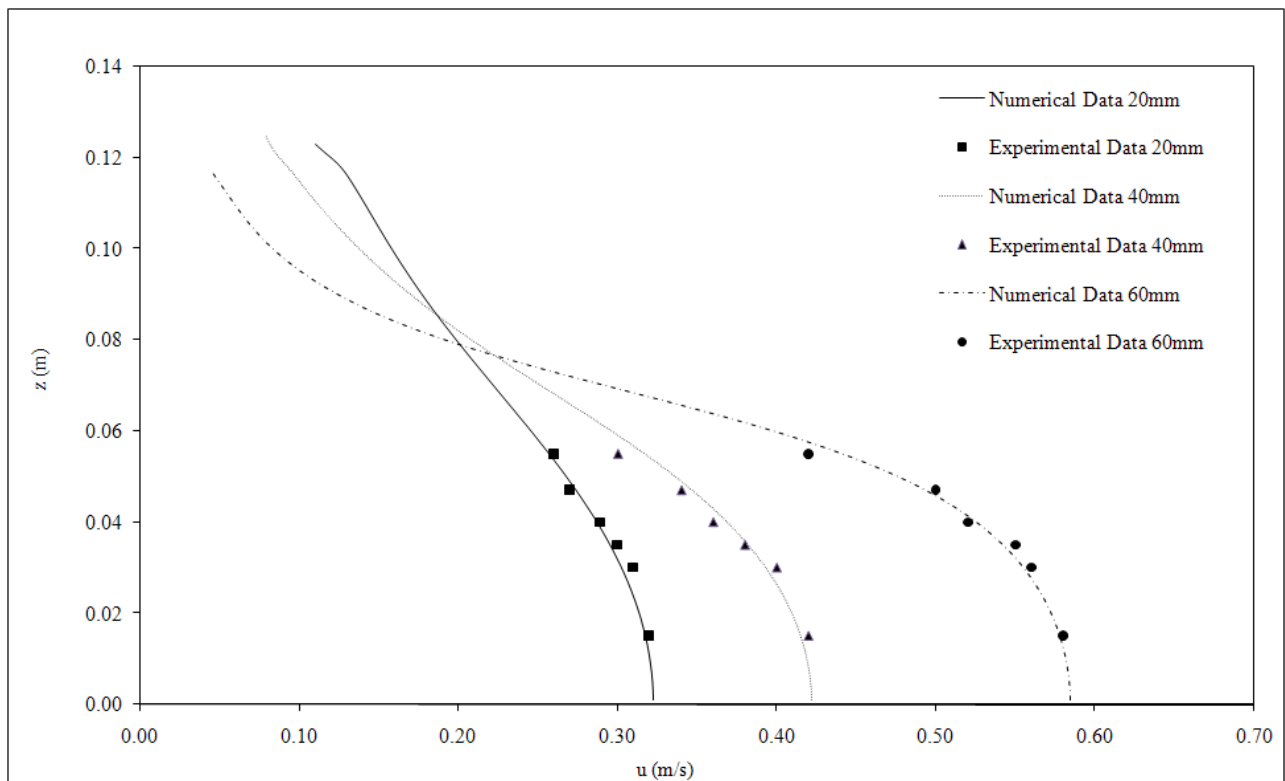


Figure 8. Comparison of experimental and numerical velocity profiles upstream to the gate at distances of (a) 60 mm, (b) 40 mm and (c) 20 mm

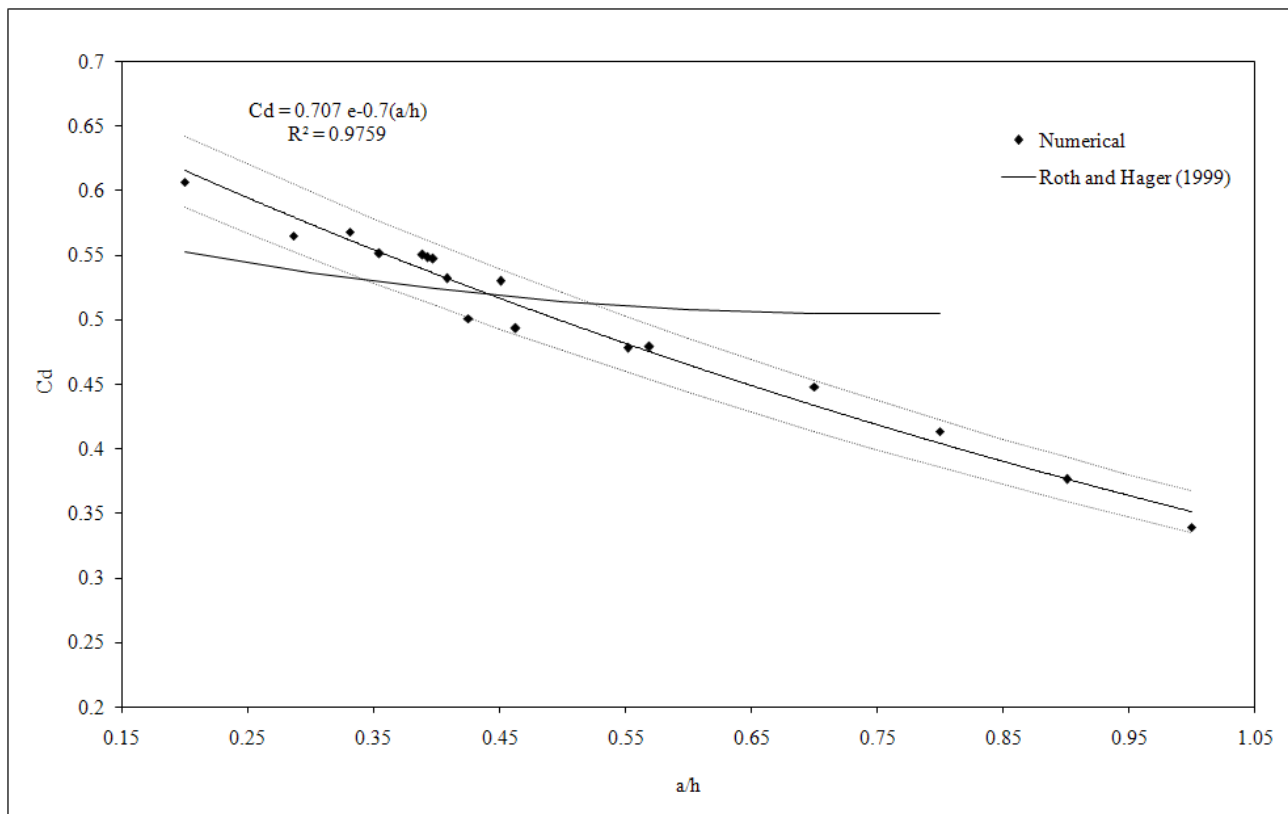


Figure 9. Numerical values of C_d vs a/h and $\pm 4.5\%$ uncertainty band ($45^\circ \leq \theta \leq 90^\circ$, $0,2 < a/h < 1,0$, $1 \leq b/a \leq 2,84$)

CONCLUSION

Experimental observations of the 3-D underflow of a sluice gate at a channel inlet allowed computation of discharge coefficients C_d as a function of relative gate opening a/h , shape ratio b/a and angle θ in a small range of a/h ($a/h = 0.28$ to 0.56); regression analysis showed that b/a and θ scarcely influence the flow and an equation was found for C_d as a function of a/h only. This equation shows a different behaviour from the well-known 2-D underflow of a sluice gate. In order to widen the experimental field, a CFD model was used; this proved to be able to simulate the flow including details as oblique wavefronts into the channel and recirculation zone upstream to the gate. Simulated discharges and water depths are very close to the observed ones; this is true also for the velocity profiles, even though they were observed in a few positions only. The results showed that viscosity effects are negligible, due to the small importance of energy losses. The CFD model was used to simulate relative openings a/h between 0.2 and 1.0 and a regression equation was finally obtained for use in practical cases.

REFERENCES

- Alfonsi G, Lauria A, Primavera L. (2012). Flow structures around a large-diameter circular cylinder. *Journal of Flow Visualization and Image Processing*. 19 (1):15-35.
- Akoz MS, Kirkgoz M S, Oner A A. (2009). Experimental and numerical modeling of a sluice gate flow. *Journal of Hydraulic Research*. 47(2):167- 176.
- Calomino F, Miglio A, Palma G, Lauria A. (2007). Discharge coefficients for sluice gates in weirs, Proc. Int. Conf. XXXII IAHR CONGRESS, Venezia (Italy).
- Cisotti U. (1908). Vene fluenti. *Rendiconti del circolo matematico di Palermo*. Palermo, Italy.
- FLOW SCIENCE (2004). FLOW-3D user manual: Excellence in flow modeling, software version 9.1. Flow Science, Inc., Santa Fe, N.M, USA.
- Gentilini B. (1941). Efflusso dalle luci soggiacenti alle paratoie piane inclinate e a settore. *L' Energia Elettrica*. 18(6), 361-380.
- Henderson F M. (1966). *Open Channel Flow*. The Macmillan Company, New York, Library of Congress catalog card number 66-10695
- Henry H R. (1950). Discussion of 'Diffusion of submerged jets' by Albertson, M.L. Y.B. Dai, R.A. Jensen and H. Rouse. *Trans ASCE* 115: 687-694.
- Hirt C W, Nichols B D. (1981). Volume of Fluid (VOF) Method for the Dynamics of Free Boundaries. *J. Comp. Phys.*, 39, 201.
- Kim D G. (2005). Contraction and discharge coefficient of free flow past a sluice gate. Proc. Int. Conf. XXXI IAHR CONGRESS, Seoul Korea, 10.
- Kim D G. (2007). Numerical Analysis of Free Flow Past a Sluice Gate, *ASCE*. 11(2), 127 – 132.
- Lauria A. (2008). Efflusso da luce di fondo di una traversa per laminazione delle piene. *Analisi sperimentale e modellazione numerica 3D*. Ph.D. Thesis. Università della Calabria, Rende, Italy.
- Marchi E. (1953). Sui fenomeni di efflusso piano da luci a battente. *Annali di Matematica Pura e Applicata*. Bologna, Italy.
- Montes J S. (1997). Irrotational flow and real fluid effects under planar sluice gates. *J. Hydraulic Eng.* 123(3), 219 – 232.
- Nago H. (1984). Scale Effects in Modeling Hydraulic Structures. H. Kobus, Esslingen am Neckar, Germany.
- Oskuyi N, Salmasi F. (2012). Vertical Sluice Gate Discharge Coefficient. *Journal of Civil Engineering and Urbanism*. 2(3): 108-114
- Rajaratnam N, Subramanya K. (1967). Flow equation for the sluice gate. *J. Irrigation and Drainage Eng.* 93(3), 167-186.
- Raju R. (1984). Scale effects in analysis of discharge characteristics of weir and sluice gates. Kobus, Esslingen am Neckar, Germany.
- Roth A, Hager W H. (1999). Underflow of standard sluice gate. *Experiments in Fluids*. 27(4), 339 – 350.